
Completion vs Optimality: Policy Gradient in Long-Horizon Cumulative-Damage Problems

Wolfgang Maass

Saarland University & German Research Center for Artificial Intelligence (DFKI)
wolfgang.maass@iss.uni-saarland.de

Sabine Janzen

German Research Center for Artificial Intelligence (DFKI)
sabine.janzen@dfki.de

Abstract

Long-horizon decision problems with cumulative damage couple locally attractive actions to globally adverse outcomes. We identify two orthogonal failure modes for policy-gradient methods on this class and propose a decomposition that separates them: *completion* (reaching the terminal horizon rather than exiting via an implicit terminal constraint) and *optimality* (matching the dynamic-programming reference given completion). Under PPO with a linear soft penalty, granting horizon access alone reduces the completion rate: the penalty’s equilibrium drives the dominant-activity share to zero, while action-space restriction combined with horizon access achieves completion but leaves an optimality gap ($\Delta M_{\text{final}} = 0.271$) that we trace to first-phase greedy commitment at the damage origin. We derive four testable predictions and evaluate them in two separately calibrated environments that share the same abstract structure but differ in domain, horizon, activity set, and calibration data: a 49-step bricklayer career and a 20-season NBA power-forward career. All four predictions replicate qualitatively. The horizon-invariance prediction is met at three of four tested horizons, with the exception at $H = 15$ consistent with the H^* boundary ($H^* \in [6, 14]$ under the NBA parameters).

1 Introduction

Many sequential decision problems accumulate state over long horizons in a way that couples locally attractive actions to globally adverse outcomes. A clinician dosing a chronic medication, an engineer scheduling heavy-duty use of a wearing component, and a worker allocating physical effort across a decades-long career all face the same structural challenge: the action that maximises immediate reward increments a cumulative state whose eventual level terminates the episode. Whether a policy-gradient agent [Schulman et al., 2017] can learn the prudent policy in such problems is a question about credit assignment over horizons that exceed any rollout-based learner’s experience. Recent long-horizon credit-assignment work [Arjona-Medina et al., 2019, Harutyunyan et al., 2019] has identified the structural difficulty but not the specific failure mode that greedy credit assignment induces when the damage signal is implicit in the terminal condition.

The diagnostic gap. A policy with low return on a long-horizon cumulative-damage problem may be failing for either of two unrelated reasons. A policy that terminates early through the implicit terminal constraint has low return because it never reaches late-horizon states. A policy that reaches the terminal horizon but commits to locally greedy actions has low return because it fails to

preserve the cumulative state. Each failure mode calls for a different intervention: horizon access addresses the former, while credit assignment targets the latter. A return-based evaluation, however, conflates both onto a single scalar, forcing a choice between diagnosing *why* the policy exits early and diagnosing *how suboptimal* it is given that the episode completes, even when both failures are present simultaneously and require separate remedies.

This paper. We evaluate policies on two independent axes. *Completion* is whether the policy reaches the terminal horizon. *Optimality* is whether the policy matches the fixed-share dynamic-programming reference [Puterman, 1994] given completion. When the constraint is *implicit* in the terminal condition, no per-step cost is available, unlike in standard CMDPs [Altman, 1999, Achiam et al., 2017, Chow et al., 2018, García and Fernández, 2015, Ray et al., 2019], and the standard decomposition does not apply. A principled evaluation requires making both failure modes separately visible. For the optimality axis we provide an analytical account: in Appendix B we derive, on a minimal cumulative-damage MDP, a sufficient condition under which the *expected* first policy-gradient update at the damage origin points toward the greedy action (Proposition 1). The proposition governs a binary-action skeleton. Its connection to the multi-activity testbeds is structural analogy and motivating context, not formal derivation. We evaluate in two environments (a 49-step bricklayer career and a 20-season NBA power-forward career) sharing the abstract structure of §3 but differing in activity set, horizon, load model, and calibration data. In both, PPO on the real environment fails completion. A Dyna [Sutton, 1990] variant with horizon access and restricted action space achieves completion but fails optimality; backward induction achieves both.

Contributions.

- A formalisation of the horizon-mismatched cumulative-damage problem class (§3), covering latent damage state, delayed proxy signal, dominant-activity structure, and implicit role-viability constraint, together with the completion-vs-optimality decomposition (§3.2).
- An empirical three-way comparison (PPO-real, fixed-share Dyna, fixed-share dynamic programming) that separately quantifies completion and optimality gaps in two environments ($\Delta M_{\text{final}} = 0.271$ bricklayer, 0.150 NBA; 95% bootstrap CI [0.148, 0.151]).
- A causal analysis showing that, under PPO with a linear soft penalty, horizon access alone is harmful (mean exit age 24.7 vs 27.8, $p = 0.028$) and action-space restriction is the intervention that unlocks completion (§5).
- A basin-of-attraction analysis identifying first-phase greedy commitment as the optimality-failure mechanism, with basin entry within the first 1% of training regardless of horizon length (§6).

2 Related Work

Constrained MDPs and safe RL. The constrained-MDP formulation [Altman, 1999] and its variants [Achiam et al., 2017, Chow et al., 2018] treat the constraint as an explicit, per-step observed quantity. Safe-exploration methods [García and Fernández, 2015, Ray et al., 2019] treat safety violations as continuous costs throughout the rollout. Our setting differs structurally: the terminal condition functions as the constraint, discovered from rollouts rather than given as a running cost, so standard CMDP methods cannot diagnose the completion failure we identify.

Policy-gradient convergence. A recent theoretical line [Mei et al., 2020, Agarwal et al., 2021, Bhandari and Russo, 2024] characterises non-convex basins in policy space. Our step-0 basin entry instantiates this regime at the damage-state origin, where immediate reward dominates the Lipschitz tail of the continuation value. Proposition 1 is derived from first principles on a minimal binary-action MDP. Its connection to the general convergence literature is structural analogy, not formal derivation. This literature speaks to our optimality axis but is silent on completion, typically assuming fixed horizons.

Long-horizon credit assignment, reward shaping, and offline methods. Methods that rebind credit to earlier actions [Harutyunyan et al., 2019, Arjona-Medina et al., 2019] target a mechanism that can bind either axis. Our decomposition isolates *which* axis is the binding constraint. Potential-based reward shaping [Ng et al., 1999] can alter the gradient landscape near initialisation. Return-conditioned methods such as Decision Transformer [Chen et al., 2021] might select trajectories

avoiding early termination but require demonstrations and inherit distribution-shift problems in the sparse late-horizon regime. Neither class is evaluated here.

Afferent signal design. The proxy signal S_t used in the testbeds is a fixed sensitisation function calibrated to epidemiological data. An alternative not pursued here is to learn or evolve the afferent signal end-to-end rather than fixing it. The proxy irrelevance finding (§5) is a diagnostic of what fixed afferents cannot provide, and whether adaptive afferent architectures close this gap without action-space restriction is an open question.

3 Problem Class, Decomposition, and Algorithmic Analysis

3.1 Problem class

We study finite-horizon MDPs with cumulative damage, specified by $(\mathcal{S}, \mathcal{A}, T, r, H, \mathcal{E})$, where \mathcal{S} contains a *cumulative damage variable* $D_t \in [0, 1]$ ($D_{t+1} = D_t + f(s_t, a_t)$, $f \geq 0$) and a *secondary preservation variable* $M_t \in [0, 1]$, $M_0 = 1$; reward is locally maximised by actions with $f(s_t, a_t) > 0$; and \mathcal{E} is a set of terminal conditions that exit the episode when cumulative damage crosses a state-dependent threshold or when role-viability is violated. The key distinction from standard CMDPs [Guin and Bhatnagar, 2022, Wachi et al., 2024] is that the constraint in \mathcal{E} is *never observed as a running cost*: the learner discovers the terminal boundary only by reaching it. We call such a problem *horizon-mismatched* when the greedy policy’s effective episode length is strictly less than H .

Assumption 1 (Cumulative-damage structure). *A cumulative-damage MDP \mathcal{M} satisfies: (i) **Monotone damage**: $f(s, a) \geq 0$ for all (s, a) , so D_t is non-decreasing along any trajectory. (ii) **Greedy-damage alignment**: the reward-maximising action satisfies $f(s, \arg \max_a r(s, a)) > 0$. (iii) **Implicit terminal boundary**: \mathcal{E} is non-empty and is avoided with positive probability only by policies under which the greedy action is not always selected.*

Beyond Assumption 1, the instances we study share five structural features. The first two concern what the agent observes and the structure of its action space: (a) **latent damage state**: D_t and the secondary preservation variable M_t are unobserved; the agent receives only a proxy signal $S_t = g(D_t)$ that is uninformative at the low-damage levels the greedy policy visits, and therefore no observation-based warning reaches the agent before the implicit boundary. We use a fixed sensitisation function calibrated to epidemiological data as a diagnostic baseline. (b) **dominant-activity structure**: one activity is simultaneously the unique reward maximiser and the unique damage maximiser, with $k - 1$ lower-reward, lower-damage alternatives creating a substitution structure whose unconstrained optimum conflicts with the role-viability constraint (c). The remaining three govern how the environment enforces and penalises damage: (c) **role-viability constraint**: the episode terminates if the trailing-window dominant-activity share falls below α , operating in the share dimension of the action space; (d) **capacity-damage feedback**: per-step reward is suppressed by $h(D_t, S_t)$, silent below D_{clin} and progressive above it; and (e) **self-amplifying secondary channel**: M_t degrades at an accelerating rate below $M_{\text{amp}} = 0.6$, making early maximum-effort trajectories irreversibly worse than proactive low-effort ones. Without (e) the optimality gap vanishes: DP and the greedy policy produce similar M_{final} at matched career lengths; both testbeds use $M_{\text{amp}} = 0.6$.

3.2 The completion-vs-optimality decomposition

Definition 1 (Completion). *A policy π achieves completion if the probability of reaching any element of \mathcal{E} before step H is zero: the expected episode length equals H .*

Definition 2 (Optimality). *Given completion, a policy π achieves optimality if $V^\pi(s_0) = V^{\pi^*}(s_0)$, where π^* is the backward-induction reference optimised over the same action subspace as π . Optimality is undefined for policies that fail completion.*

These definitions induce a three-outcome ordinal scale (Table 1). The *optimality gap* is $\Delta M_{\text{final}} = M_{\text{final}}^{\text{DP}} - M_{\text{final}}^\pi$. Definition 2 is stated in terms of V^π . ΔM_{final} serves as a domain-specific surrogate for the value gap, justified by feature (e): under the self-amplifying secondary channel and the fixed-share constraint, M_{final} is a monotone function of V^π given completion, so $V^\pi < V^{\pi^*} \Leftrightarrow M_{\text{final}}^\pi < M_{\text{final}}^{\pi^*}$. Accordingly, $\Delta M_{\text{final}} = 0$ corresponds to Cell C and $\Delta M_{\text{final}} > 0$ to Cell B.

Table 1: Three-outcome scale induced by Definitions 1 and 2. The scale is strictly ordered Cell A \prec Cell B \prec Cell C. Optimality is only meaningful once completion is achieved; Cell A vs. Cell B/C comparisons on M_{final} confound truncation with suboptimality and are not made in this paper.

Cell	Completion	Optimality
A	fails	undefined (episode truncated before late-horizon states; M_{final} artificially high)
B	achieves	fails ($V^\pi < V^{\pi^*}$, optimality gap > 0)
C	achieves	achieves ($V^\pi = V^{\pi^*}$, optimality gap = 0)

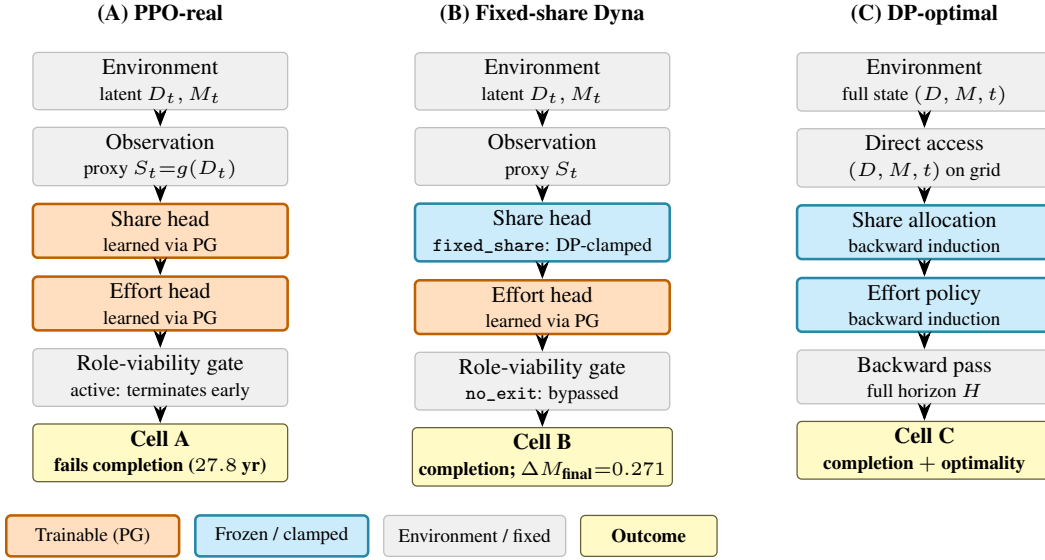


Figure 1: Three-way method-comparison architecture. Columns share the pipeline state \rightarrow observation \rightarrow share/effort heads \rightarrow role-viability gate \rightarrow outcome and differ only in which components are trainable (orange) vs. clamped (cyan). `fixed_share` replaces the trainable share head; `no_exit` bypasses the role-viability gate.

3.3 Mechanism analysis: backward induction vs. policy gradient

Backward induction achieves both axes. DP evaluates every (D, M, t) grid point backward from H , and therefore \mathcal{E} is avoided *a priori* and the capacity-damage feedback (d) is integrated over the full remaining horizon. At $(D_0 = 0, M_0 = 1, t = 0)$, sustained low effort is identified as the unique trajectory keeping D below D_{clin} . Latent state (a) is moot under direct grid access (Figure 1, column C).

Policy gradient fails completion. Under Assumption 1(ii)–(iii), the greedy policy reaches \mathcal{E} before H . When horizon access is granted via `no_exit`, the linear soft penalty’s per-step cost outweighs the dominant activity’s reward advantage, and therefore the share head’s unconstrained optimum places mass at zero on the dominant activity, violating the constraint the hard exit would have enforced. Completion failure arises from two interacting causes: the implicit terminal boundary and the uninformative afferent in the greedy policy’s operating damage range, addressable via action-space restriction (`fixed_share`, studied here) or by improving the afferent’s informativeness in the policy’s operating damage range. Clamping shares to a constraint-satisfying allocation structurally prevents role-viability violations regardless of whether horizon access is granted.

Policy gradient fails optimality. Even with completion achieved, the dominant-activity structure (b) creates a first-phase commitment at $D = 0$: the reward gap $e_H^\beta - e_L^\beta$ is large while damage cost is zero, and therefore the first policy-gradient update (in expectation) commits to maximum effort on the dominant activity. Proposition 1 (Appendix B) formalises this as a sufficient condition on the

Table 2: Bricklayer instantiation of Table 1. Cell A M_{final} omitted (truncation confounds with suboptimality). † career ends at age 65 ($H = 49$ steps).

Condition	Cell	Seeds	Exit age (mean \pm sd)	Completion	Optimality
PPO-real	A	20	27.8 \pm 4.0	fails	—
Unrestricted Dyna	A	20	24.7 \pm 4.5	fails	—
Fixed-share Dyna (dom.)	B	8/10	65.0 \pm 0.0	achieves	fails
DP-optimal	C	—	65 [†]	achieves	achieves

expected gradient direction in a binary-action minimal MDP. The self-amplifying channel (e) then ensures that once M falls below M_{amp} , the degradation cascade is irreversible.

3.4 Testable predictions

The analysis of §3.3 yields four testable predictions about any cumulative-damage MDP satisfying Assumption 1 with features (a)–(e), under PPO with a linear soft penalty for the completion-axis predictions (P1–P2). The proxy signal (a) contributes nothing detectable to completion because its informative range ($D > D_{\text{clin}}$) is disjoint from the greedy policy’s operating damage range (confirmed empirically in §5). Backward induction achieves both axes by construction and occupies Cell C; it serves as the upper-bound reference throughout.

- P1 PG-real fails completion.** Policy gradient trained on real rollouts with \mathcal{E} enforced exits early, occupying Cell A.
- P2 Horizon access alone is harmful** (under PPO with linear soft penalty): granting horizon access without action-space restriction shortens careers relative to PG-real, because the penalty’s equilibrium under (c) drives the dominant-activity share below α .
- P3 Reactive-decline attractor.** Under completion and given the self-amplifying structure (e), the dominant attractor is maximum effort at $t = 0$, monotone decline, M irreversibly below M_{amp} , and positive ΔM_{final} .
- P4 Horizon invariance.** The reactive attractor’s dominance rate and ΔM_{final} are invariant across training horizons $H \leq H^*$, because basin entry occurs at step 0.

4 Testbeds and Headline Results

We test P1–P4 in two cumulative-damage environments. Both satisfy Assumption 1 and features (a)–(e) but differ in activity set, horizon, load model, biological calibration data, and role-viability parameters. The two environments share the same simulation engine, the HMS regulation pathway, and the Baratz amplification function. The replication therefore tests whether the findings generalise across parameter regimes of the same problem class, not across independently developed simulators, a limitation we return to in §8.

The **bricklayer** testbed models a 49-year career over $k = 7$ construction activities, calibrated to a bio-physical model of the human knee [Coggon et al., 2000, Jensen, 2008, Rytter et al., 2009, Baratz et al., 1986, Arendt-Nielsen et al., 2010] (Appendix C). The **NBA power-forward** testbed models a 20-season career over 6 activities, calibrated to the sports-medicine literature [Drakos et al., 2010, Wiggins et al., 2016] (Appendix G).

Figure 2 and Table 2 summarise the headline three-way contrast. The DP reference is computed in under two hours on a single CPU (Appendix D), and the gap cannot therefore be attributed to the cost of computing the DP reference.

5 Completion: Causal Analysis

PPO-real fails completion (P1). PPO with $\gamma = 1$ (undiscounted episodic return; the rbar exponential moving-average baseline of Mahadevan 1996 is used for variance reduction) terminates at a mean age of 27.8 ± 4.0 years, with 100% of 2,000 eval episodes ending in role-violation (20 seeds,

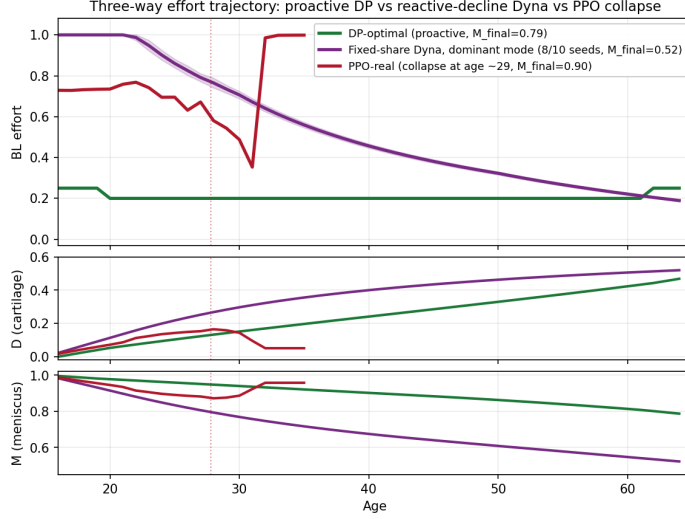


Figure 2: Three-way dominant-activity effort (bricklayer, $H = 49$). DP-optimal (green, Cell C, $M_{\text{final}}=0.79$); dominant-mode Dyna (purple, Cell B, 8/10 seeds, 0.52); PPO-real (red, Cell A, exit ≈ 27.8 yr). Headline gap $\Delta M_{\text{final}} = 0.271$.

10 curriculum-on and 10 curriculum-off). The role-viability rule fires when

$$\frac{1}{W} \sum_{\tau=t-W+1}^t s_{\text{dom}}^{(\tau)} < \alpha,$$

with $W = 5$ years and $\alpha = 0.15$ in the bricklayer. The agent observes only the proxy signal S_t . The trailing share history $s_{\text{dom}}^{(\tau)}$, $\tau \in [t-W+1, t-1]$ that determines the role-viability boundary is not provided in the state observation, making the constraint boundary non-Markovian from the agent’s perspective. This partial-observability challenge is a contributing factor to PPO-real’s failure, separate from and additional to the long-horizon credit-assignment difficulty. Each is acknowledged in the Limitations of §8. Including the proxy signal S in the state yields $\Delta = -0.65$ yr relative to zeroing it (20 seeds per condition), within seed variance and in the wrong direction: S becomes informative only at $D > 0.3$, whereas PPO-real exits at $D_{\text{final}} = 0.16$. The proxy is not uninformative in principle. It is informative about states the learner never reaches, a diagnostic of the fixed afferent’s design, which covers the clinical damage range rather than the early-career range where the greedy policy operates.

Horizon access alone is harmful (P2). Across 20 seeds of the best unrestricted Dyna configuration, trained with rollouts extended past role-violation (`no_exit` flag) and a linear soft role penalty with weight $w = 1.0$ (applied as $-w \cdot \mathbf{1}[s_{\text{dom},t} < \alpha]$ per step), the mean exit age under real evaluation is 24.7 years (95% CI [23.0, 26.8]), *earlier* than PPO-real’s 27.8 (Welch’s $t(37.8) = -2.29$, $p = 0.028$; Mann-Whitney $p = 0.009$). The exit-age distribution is bimodal: 10/20 seeds exit at age 21 via role-violation (the earliest age the trailing-window check can fire); the remaining 10 seeds survive to ages 26–38. The linear soft penalty does not induce an interior basin around any positive dominant-activity allocation, and therefore the share head’s unconstrained optimum places mass at zero once curriculum scaffolding lifts. Whether convex or entropy-regularised alternatives escape this pattern is open (§8).

Action-space restriction unlocks completion. Restricting the policy to the DP-optimal share allocation (`fixed_share`, learning only effort) achieves completion in all cases: all 10 seeds reach the terminus (65.0 ± 0.0 yr, zero role-violations over 1,000 eval episodes) across $H \in \{13, 20, 30, 49\}$ (Appendix A). Completion is a function of action-space structure, not horizon length.

Fixed-share PPO-real ablation. To isolate whether action-space restriction alone (without `no_exit`) suffices, we run `fixed_share` PPO-real with the role-viability gate active during training

(10 seeds). All 10 seeds achieve 100% completion (exit age 65.0 ± 0.0). Completion is therefore attributable to the structural share constraint, which keeps $s_{\text{dom}} \geq \alpha$ by construction. `no_exit` is not independently necessary for completion but is required for the Dyna agent to accumulate long-horizon experience.

A (W, α) sensitivity sweep (90 runs, Appendix F) confirms threshold robustness.

6 Optimality: Basin Analysis

6.1 Reactive decline is the dominant attractor (P3)

Across 10 seeds of the fixed-share Dyna sweep, 8 converge to a nearly identical effort profile: maximum effort at $t = 0$, monotone decline to 0.22 by age 60 (Figure 3b). Seed-to-seed variance in dominant-mode M_{final} is 0.001, three orders of magnitude tighter than the gap to DP-optimal, confirming this is a distinct fixed point, not optimisation noise.

The mechanism is feature (e): early maximum effort drives M below $M_{\text{amp}} = 0.6$ irreversibly, triggering a degradation cascade the DP avoids by sustaining low effort from $t = 0$. Two seeds escape the reactive basin: seed 4 via an inverted-U effort profile ($M_{\text{final}} = 0.64$) and seed 7 via a mid-training reward collapse to a DP-like low-effort mode ($M_{\text{final}} = 0.825$), demonstrating that the DP-competitive region is stochastically reachable, though not via a reliable convergence path. The basin-dominance claim is accordingly about 8 of 10 seeds (95% Clopper–Pearson CI $[0.44, 0.97]$), not 10 of 10.

6.2 First-phase basin entry as the mechanism (P4)

Three pieces of evidence support first-phase basin entry:

1. **All 8 dominant-cluster seeds reach maximum effort at the initial state within the first 10,000 training steps** ($\approx 1\%$ of training), read from periodic training logs. The reactive trajectory is established before any long-horizon signal has accumulated.
2. **The two escaping seeds did not commit at step 0.** Seed 4 has initial-state effort 0.183 and seed 7 has 0.346; both escaped because their stochastic first gradient update did not push toward the maximum. Proposition 1 governs the *expected* gradient direction. Individual sample gradients can differ in sign, which is consistent with these two escaping seeds.
3. **The basin structure is invariant to training horizon** across $H \in \{13, 20, 30, 49\}$: dominant-mode M_{final} is constant at 0.523 ± 0.001 regardless of horizon (Appendix A, Figure 4). A basin entered by aggregating long-horizon signals would shift with H . This one does not.

Proposition 1 (Appendix B) formalises the *direction of the expected gradient* in a binary-action minimal MDP. The empirical evidence above establishes saturation within the first 1% of training for all 8 reactive-cluster seeds.

6.3 Initialization intervention: a falsifiability test

The first-phase account predicts that biasing the effort head’s initial output toward the DP-optimal value weakens the basin’s dominance. Setting the effort head’s final-layer bias to -1.386 ($\sigma(-1.386) \approx 0.20$, matching DP-optimal sustained effort), with all other settings identical to the fixed-share sweep, produces **4/10 seeds escaping** (vs. 2/10 baseline) and raises mean M_{final} from 0.564 to 0.609.

Pre-registered binding thresholds (prompts/e1_prereg.md, frozen 2026-04-20): ≥ 6 confirms, 4–5 is *nuanced*, ≤ 3 falsifies. The result falls in the nuanced band. Six seeds revert to the reactive basin within the first 10^4 gradient updates. The four escapers split into three attractor types: seeds 4 and 7 reach DP-competitive $M_{\text{final}} \in [0.79, 0.85]$; seed 9 converges to near-zero late-career effort ($e_{t>40} \approx 0$); seed 0 oscillates. Per-seed results are in Appendix D, Table 5). Seeds 4 and 7 represent qualitatively distinct effort profiles: seed 4 converges to a gradually increasing schedule near the DP-optimal level, while seed 7 settles below the DP grid minimum ($e < 0.20$) and achieves $M_{\text{final}} = 0.846$, exceeding the DP reference. Both escape the reactive basin not by resolving the

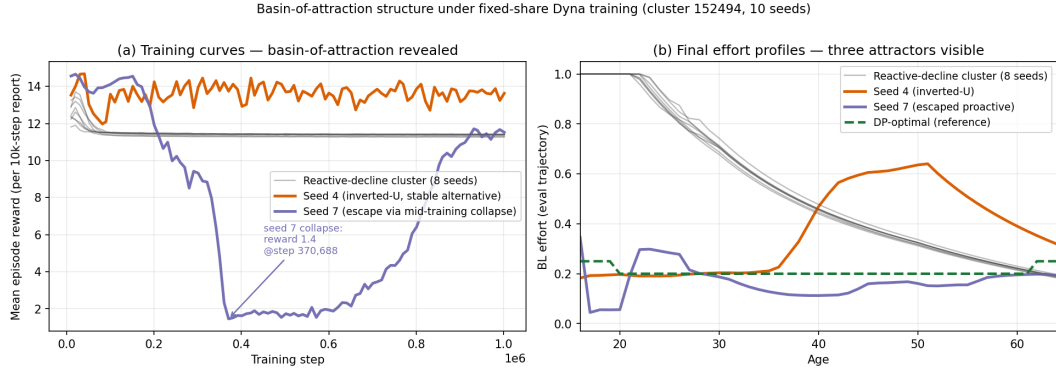


Figure 3: Basin-of-attraction structure (10 seeds, bricklayer). (a) 8 seeds converge to the reactive-decline attractor ($\sim 100k$ steps); seed 4 reaches a stable alternative; seed 7 collapses mid-training and partially recovers, demonstrating that the DP-competitive region is stochastically reachable. (b) Final effort profiles; all 8 reactive seeds output maximum effort after only 10k steps.

long-horizon credit-assignment problem but by avoiding step-0 commitment, a pattern consistent with the occupational health finding that conservative early-career effort profiles produce better long-run outcomes than maximum early effort [McLellan et al., 2022]. The attraction is strong but not absolute: closing the gap requires weakening the basin’s attraction, not correcting the initialisation.

7 Replication: NBA Career Environment

To distinguish the bricklayer findings from parameter-specific artefacts, we replicate the four-condition experiment in the NBA power-forward testbed (§4).

Completion axis (P1–P2) replicates. PPO-real fails across all 20 seeds (exit 22.6 ± 1.8 , role-violation 100%). Unrestricted Dyna across 60 seeds ($w \in \{0.5, 1.0, 2.0\}$) exits at 21.2 yr, 1.4 yr earlier than PPO-real ($p = 0.003$ Welch’s t ; $p = 0.0003$ Mann-Whitney). The same direction of harm confirms the mechanism is not domain-specific. Fixed-share Dyna achieves 100% completion (10/10 reach age 38).

Optimality axis (P3–P4) replicates with compression. $\Delta M_{\text{final}} = 0.150$ (95% CI [0.148, 0.151]), above the pre-registered 0.10 threshold. The NBA testbed falls outside the analytical guarantee ($H^* \in [6, 14]$, Appendix B), providing a direct test of whether the commitment condition is sufficient but not necessary: the reactive basin is the plurality attractor (4/10) rather than the bricklayer’s majority (8/10), consistent with the H^* compression prediction. Three seeds settle in a mid-cluster ($M_{\text{final}}=0.71$) and three converge near DP (0.85). Fisher’s exact $p = 0.17$ at $n = 10$ is non-significant per-environment, but the decomposition generalises across domains.

Horizon invariance (P4) replicates at 3 of 4 horizons. Dominant-mode M_{final} is 0.614, 0.614, 0.648, 0.615 for $H = 7, 10, 15, 20$. Three horizons agree to within 0.001; the $H = 15$ outlier is consistent with H^* in [6, 14] (Appendix B): $H = 15$ lies outside the analytical guarantee under both damage channels. The basin-dominance rate decreases as H exceeds H^* . The step-0 mechanism remains universal.

8 Discussion

The decomposition as diagnostic. The decomposition separates two failure modes that return-based evaluation conflates, and shows that interventions targeting one axis can worsen the other: a paper reporting only exit age would claim fixed-share Dyna is solved, while one reporting only M_{final} would be misled by PPO-real’s artificially high (early-exit) score. The decomposition also maps existing interventions to the axis each addresses. Action-space restriction (`fixed_share`) targets the completion axis by enforcing a constraint-satisfying share allocation. Improving the

Table 3: Bricklayer ($H = 49$) vs. NBA ($H = 20$) replication summary.

Finding	Bricklayer	NBA
PPO-real completion rate	0%	0%
PPO-real mean exit age	27.8 ± 4.0	22.6 ± 1.8
Unrestr. Dyna Δ exit vs PPO-real	-3.1 yr	-1.4 yr
Welch’s t (p) / Mann-Whitney (p)	0.028 / 0.009	0.003 / 0.0003
Fixed-share Dyna completion rate	100%	100%
$M_{\text{final}}^{\text{DP}}$	0.794	0.764
$M_{\text{final}}^{\text{Dyna,dom}}$	0.523 ± 0.001	0.614 ± 0.002
ΔM_{final} (95% CI)	0.271	0.150 [0.148, 0.151]
Reactive-basin dominance (95% CP CI)	8/10 [0.44, 0.97]	4/10 [0.12, 0.74]
Fisher exact (p , dominance difference)	$p = 0.17$; not significant at $n = 10$	

afferent’s informativeness in the policy’s operating damage range targets the completion axis from the information side. The optimality gap ($\Delta M_{\text{final}} = 0.271$) remains open to both interventions and requires a separate credit-assignment solution. The reactive-decline policy is qualitatively consistent with occupational epidemiology [Palmer, 2012, Coggon et al., 2000, Jensen, 2008, Rytter et al., 2009]: workers maintain high effort until tissue damage forces reactive regulation [Woolf and Salter, 2000, Arendt-Nielsen et al., 2010], though real workers face financial and social constraints we do not model. We conjecture the failure modes generalise to other cumulative-damage domains satisfying Assumption 1 with features (a)–(e).

Connection to early sport specialisation. The reactive-decline attractor has a direct empirical counterpart in the early sport specialisation literature [DiFiori et al., 2014, McLellan et al., 2022, Jildev, 2024]: maximum dominant-activity effort from career outset, accelerating secondary degradation once a tissue threshold is crossed, and premature exit. The structural parallels are precise: latent damage accumulation before pain signals become informative (feature (a)), self-amplifying degradation below M_{amp} (feature (e)), and implicit role-viability violation as the terminal condition. Empirically, NBA players who specialised in a single sport during adolescence play in fewer career games and suffer more serious injuries than multi-sport athletes [McLellan et al., 2022], consistent with the model’s prediction that distributing effort across activities preserves M_{final} . The step-0 commitment mechanism provides a formal account of why agents in this class converge to this pattern even when proactive load management would be optimal.

Limitations. *Same engine:* replication tests parameter-regime generality within one codebase, not across independently developed simulators. *Proposition–testbed gap:* Proposition 1 covers a binary-action minimal MDP; it motivates but does not formally derive the empirical findings in the multi-activity continuous-effort testbeds. *PPO and penalty specificity:* whether convex penalties or maximum-entropy methods (SAC, Haarnoja et al., 2018) escape harmful horizon access is open. *Ground-truth model:* Dyna uses the exact simulator transition; practical model-based RL incurs additional misspecification error. *Partial observability:* the role-viability boundary depends on the trailing W -step share history, which is absent from the state observation, making the constraint non-Markovian from the agent’s perspective. *Shared trunk:* the share and effort heads share a common network trunk; a two-trunk architecture would provide stricter causal isolation of the two failure modes.

Broader impact and future directions. The framework can inform ergonomic interventions extending productive working life; risks of discriminatory reuse are mitigated by population-level synthetic agents and no individual-prediction API. Priority experiments: convex share penalty ($-\lambda \log(s_{\text{dom}} - \alpha)$), non-DP-optimal share control, SAC comparison, a sweep over initial effort-head bias values to test whether the escape rate increases monotonically, replacing the fixed proxy signal with a learned or evolved internal-signal architecture, to test whether adaptive afferents restore completion without action-space restriction, and a two-trunk architecture to provide a stricter causal isolation of the share and effort failure modes.

References

- Joshua Achiam, David Held, Aviv Tamar, and Pieter Abbeel. Constrained policy optimization. In *Proceedings of the 34th International Conference on Machine Learning (ICML)*, pages 22–31, 2017.
- Alekh Agarwal, Sham M. Kakade, Jason D. Lee, and Gaurav Mahajan. On the theory of policy gradient methods: Optimality, approximation, and distribution shift. *Journal of Machine Learning Research*, 22(98):1–76, 2021.
- Barbara E. Ainsworth, William L. Haskell, Stephen D. Herrmann, Nathanael Meckes, David R. Bassett, Cathrine Tudor-Locke, Jennifer L. Greer, Jesse Vezina, Melicia C. Whitt-Glover, and Arthur S. Leon. 2011 compendium of physical activities: A second update of codes and met values. *Medicine & Science in Sports & Exercise*, 43(8):1575–1581, 2011.
- Eitan Altman. *Constrained Markov Decision Processes*. Chapman & Hall / CRC, Boca Raton, 1999.
- Lars Arendt-Nielsen, Hongling Nie, Mogens Berg Laursen, Bjarne Stengaard Laursen, Pascal Madeleine, Ole Hoejbjerg Simonsen, and Thomas Graven-Nielsen. Sensitization in patients with painful knee osteoarthritis. *Pain*, 149(3):573–581, 2010.
- José A. Arjona-Medina, Michael Gillhofer, Michael Widrich, Thomas Unterthiner, Johannes Brandstetter, and Sepp Hochreiter. RUDDER: Return decomposition for delayed rewards. In *Advances in Neural Information Processing Systems 32 (NeurIPS)*, pages 13544–13555, 2019.
- Mark E. Baratz, Freddie H. Fu, and Ronald Mengato. Meniscal tears: The effect of meniscectomy and of repair on intraarticular contact areas and stress in the human knee. *The American Journal of Sports Medicine*, 14(4):270–275, 1986.
- Jalaj Bhandari and Daniel Russo. Global optimality guarantees for policy gradient methods. *Operations Research*, 72(5):1906–1927, 2024.
- Lili Chen, Kevin Lu, Aravind Rajeswaran, Kimin Lee, Aditya Grover, Michael Laskin, Pieter Abbeel, Aravind Srinivas, and Igor Mordatch. Decision transformer: Reinforcement learning via sequence modeling. In *Advances in Neural Information Processing Systems (NeurIPS)*, volume 34, 2021.
- Yinlam Chow, Ofir Nachum, Edgar Duenez-Guzman, and Mohammad Ghavamzadeh. A Lyapunov-based approach to safe reinforcement learning. In *Advances in Neural Information Processing Systems 31 (NeurIPS)*, pages 8103–8112, 2018.
- David Coggon, Peter Croft, Stella Kellingray, Deborah Barrett, Martin McLaren, and Cyrus Cooper. Occupational physical activities and osteoarthritis of the knee. *Arthritis & Rheumatism*, 43(7):1443–1449, 2000.
- John P. DiFiori, Holly J. Benjamin, Joel S. Brenner, Andrew Gregory, Neeru Jayanthi, Gregory L. Landry, and Anthony Luke. Overuse injuries and burnout in youth sports: A position statement from the american medical society for sports medicine. *British Journal of Sports Medicine*, 48(4):287–288, 2014.
- Mark C. Drakos, Benjamin Domb, Chad Starkey, Lisa Callahan, and Answorth A. Allen. Injury in the national basketball association: A 17-year overview. *Sports Health*, 2(4):284–290, 2010.
- Javier García and Fernando Fernández. A comprehensive survey on safe reinforcement learning. *Journal of Machine Learning Research*, 16(1):1437–1480, 2015.
- Soumyajit Guin and Shalabh Bhatnagar. A policy gradient approach for finite horizon constrained Markov decision processes. *arXiv preprint arXiv:2210.04527*, 2022.
- Tuomas Haarnoja, Aurick Zhou, Pieter Abbeel, and Sergey Levine. Soft actor-critic: Off-policy maximum entropy deep reinforcement learning with a stochastic actor. In *Proceedings of the 35th International Conference on Machine Learning (ICML)*, pages 1861–1870, 2018.

- Anna Harutyunyan, Will Dabney, Thomas Mesnard, Mohammad Gheshlaghi Azar, Bilal Piot, Nicolas Heess, Hado van Hasselt, Greg Wayne, Satinder Singh, Doina Precup, and Rémi Munos. Hindsight credit assignment. In *Advances in Neural Information Processing Systems (NeurIPS)*, volume 32, 2019.
- Lilli Kirkeskov Jensen. Knee osteoarthritis: Influence of work involving heavy lifting, kneeling, climbing stairs or ladders, or kneeling/squatting combined with heavy lifting. *Occupational and Environmental Medicine*, 65(2):72–89, 2008.
- Toufic R. Jildeh. Load management is essential to prevent season-ending injuries in the national basketball association. *Arthroscopy: The Journal of Arthroscopic and Related Surgery*, 40(6):1680–1681, 2024.
- Sridhar Mahadevan. Average reward reinforcement learning: Foundations, algorithms, and empirical results. *Machine Learning*, 22:159–195, 1996.
- Maddison McLellan, Sachin Allahabadi, and Nirav K. Pandya. Youth sports specialization and its effect on professional, elite, and olympic athlete performance, career longevity, and injury rates: A systematic review. *Orthopaedic Journal of Sports Medicine*, 10(11):23259671221129594, 2022.
- Jincheng Mei, Chenjun Xiao, Csaba Szepesvári, and Dale Schuurmans. On the global convergence rates of softmax policy gradient methods. In *Proceedings of the 37th International Conference on Machine Learning (ICML)*, pages 6820–6829, 2020.
- Andrew Y. Ng, Daishi Harada, and Stuart Russell. Policy invariance under reward transformations: Theory and application to reward shaping. In *Proceedings of the 16th International Conference on Machine Learning (ICML)*, pages 278–287, 1999.
- Keith T. Palmer. Occupational activities and osteoarthritis of the knee. *British Medical Bulletin*, 102(1):147–170, 2012.
- Martin L. Puterman. *Markov Decision Processes: Discrete Stochastic Dynamic Programming*. John Wiley & Sons, Inc., New York, 1994.
- Alex Ray, Joshua Achiam, and Dario Amodei. Benchmarking safe exploration in deep reinforcement learning. Technical report, OpenAI, 2019. Safety Gym benchmark.
- Stine Rytter, Lilli Kirkeskov Jensen, Jens Peter Bonde, Anne Grethe Jurik, and Niels Egdund. Occupational kneeling and meniscal tears: A magnetic resonance imaging study in floor layers. *The Journal of Rheumatology*, 36(7):1512–1519, 2009.
- John Schulman, Filip Wolski, Prafulla Dhariwal, Alec Radford, and Oleg Klimov. Proximal policy optimization algorithms. *arXiv preprint arXiv:1707.06347*, 2017.
- Richard S. Sutton. Integrated architectures for learning, planning, and reacting based on approximating dynamic programming. In *Proceedings of the 7th International Conference on Machine Learning (ICML)*, pages 216–224, 1990.
- Henk F. van der Molen, Judith K. Sluiter, Carel T. J. Hulshof, Peter Vink, and Monique H. W. Frings-Dresen. Effectiveness of measures and implementation strategies in reducing physical work demands due to manual handling at work. *Scandinavian Journal of Work, Environment & Health*, 31(supplement 2):75–87, 2005.
- Akifumi Wachi et al. A survey of constraint formulations in safe reinforcement learning. *arXiv preprint arXiv:2402.02025*, 2024.
- Aaron J. Wiggins, Ravi K. Grandhi, Daniel K. Schneider, Denver Stanfield, Kate E. Webster, and Gregory D. Myer. Risk of secondary injury in younger athletes after anterior cruciate ligament reconstruction: A systematic review and meta-analysis. *The American Journal of Sports Medicine*, 44(7):1861–1876, 2016.
- Clifford J. Woolf and Michael W. Salter. Neuronal plasticity: Increasing the gain in pain. *Science*, 288(5472):1765–1769, 2000.

A Horizon Invariance of the Basin Structure

This appendix reports the horizon-invariance experiment supporting prediction P4 (§3.4) and the first-phase basin-entry claim of §6.2. The bricklayer fixed-share Dyna sweep was run at four training horizons, $H \in \{13, 20, 30, 49\}$, with 10 seeds per horizon and all other hyperparameters held fixed (Appendix D).

Evaluation protocol. All policies, regardless of training horizon, are evaluated on the full $H = 49$ environment. A policy trained at $H = 13$ is therefore evaluated zero-shot on the career up to age 65; its M_{final} is measured at step 48 (age 65). This ensures all four training horizons produce comparable M_{final} values. The horizon-invariance of $M_{\text{final}} = 0.523 \pm 0.001$ across all four conditions therefore cannot be attributed to differences in evaluation length.

Findings. (i) The reactive-decline basin holds 6–8 of 10 seeds at every H (Figure 4a); the dominance rate does not increase with longer training. (ii) Dominant-mode effort schedules overlap to within seed noise across the four horizons (panel b): the policy learned from 13 training years is indistinguishable from the policy learned from 49. (iii) Dominant-mode M_{final} is invariant at 0.523 ± 0.001 (panel c); the gap to DP-optimal (0.271) does not shrink with H , confirming first-phase basin entry (§6.2). NBA replication of P4 at $H \in \{7, 10, 15, 20\}$ is reported in §7.

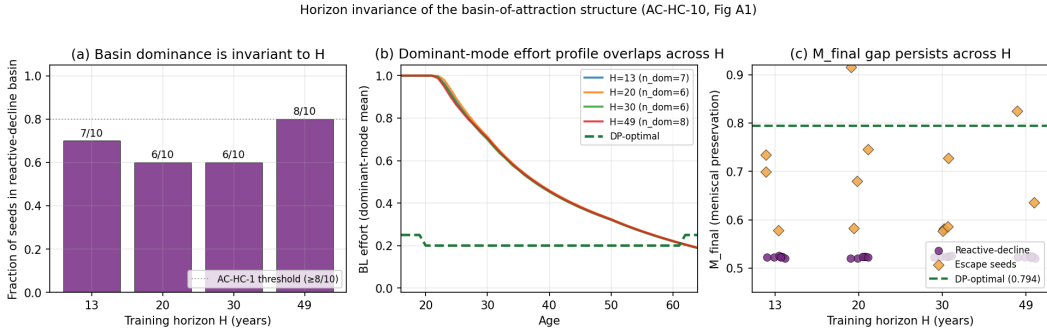


Figure 4: Horizon invariance of the basin-of-attraction structure (bricklayer testbed). All conditions evaluated on the full $H = 49$ environment. (a) Reactive-decline basin holds 6–8 of 10 seeds across training horizons $H \in \{13, 20, 30, 49\}$. (b) Dominant-mode effort profiles overlap nearly perfectly across H : the policy learned from 13 years of training rollouts is indistinguishable in effort schedule from the policy learned from 49 years. (c) Dominant-mode M_{final} is invariant across H at 0.523 ± 0.001 ; the gap to DP-optimal (0.271) does not shrink with longer training. This is direct evidence for first-phase basin entry: the reactive attractor is determined by the first policy-gradient update, not by the long-horizon signal that longer rollouts provide. Data: cluster 152494 ($H = 49$) and cluster 152523 ($H \in \{13, 20, 30\}$).

B Step-0 Basin Entry in a Minimal Cumulative-Damage MDP

This appendix derives Proposition 1 on a minimal MDP that retains only the features essential to the step-0 mechanism. The minimal MDP omits the multi-activity structure, secondary-channel amplification, and age-dependent capacity of the testbeds; it therefore speaks to the *direction of the expected first update* and the H^* boundary, not to the magnitude of ΔM_{final} or the full attractor structure.

Setup. Finite-horizon MDP with scalar damage $D_t \in [0, 1]$, $D_0 = 0$; binary effort $e_t \in \{e_L, e_H\}$, $0 < e_L < e_H \leq 1$; transition $D_{t+1} = \min(1, D_t + \kappa e_t)$; reward $r(D_t, e_t) = e_t^\beta (1 - D_t)^2$ for $\beta \in (0, 1]$; return $G(\tau) = \sum_{t=0}^{H-1} r(D_t, e_t)$. This satisfies Assumption 1 and is the skeleton on which the step-0 mechanism operates.

Lemma 1 (Lipschitz bound on V^π). *Let $\bar{e}_\beta = \frac{1}{2}(e_L^\beta + e_H^\beta)$ be the expected per-step effort reward under the uniform policy at $D > 0$. Under the deterministic transition $D_{t+1} = D_t + \kappa e_t$ (prior to*

clipping at 1), the continuation value satisfies

$$|V^\pi(\kappa e_H) - V^\pi(\kappa e_L)| \leq 2(H-1) \bar{e}_\beta \kappa (e_H - e_L).$$

Proof. The reward $r(D, e) = e^\beta(1-D)^2$ satisfies $|\partial r / \partial D| = 2e^\beta(1-D) \leq 2e^\beta$ on $[0, 1]$. Under the uniform policy for $t \geq 1$, damage evolves deterministically, so $\partial D_t / \partial D_1 = 1$ for all $t \geq 1$. The continuation value $V^\pi(\kappa e)$ covers steps $t = 1, \dots, H-1$ (i.e., $H-1$ steps). By the chain rule:

$$\left| \frac{dV^\pi}{dD_1} \right| \leq \sum_{t=1}^{H-1} \mathbb{E}[2e_t^\beta] \leq 2(H-1) \bar{e}_\beta.$$

Applying this to the gap $V^\pi(\kappa e_H) - V^\pi(\kappa e_L)$ via the mean-value theorem in D_1 gives the stated bound. \square

Policy and first-update gradient. Parameterise the $D = 0$ action distribution by $\theta \in \mathbb{R}$: $\pi_\theta(e_H | D = 0) = \sigma(\theta)$, initialised at $\theta_0 = 0$ (uniform). Action selection at $D > 0$ is held at uniform $\Pr(e_H) = 1/2$; we analyse only the first update on θ . The REINFORCE gradient is $\nabla_\theta J(\theta) = \mathbb{E}_\pi[\nabla_\theta \log \pi_\theta(a_0 | D_0) G(\tau)]$. At $\theta_0 = 0$, $\sigma(\theta_0) = 1/2$ and $\nabla_\theta \log \pi_{\theta_0}(e_H | 0) = +1/2$, $\nabla_\theta \log \pi_{\theta_0}(e_L | 0) = -1/2$. Splitting the expectation by the first action and identifying the inner expectations as $Q^\pi(0, e_H)$ and $Q^\pi(0, e_L)$ yields

$$\nabla_\theta J(\theta)|_{\theta_0} = \frac{1}{4} [Q^\pi(0, e_H) - Q^\pi(0, e_L)]. \quad (1)$$

The sign of the *expected* first update equals the sign of the state-action-value gap at $D = 0$. Using the Bellman decomposition $Q^\pi(0, e) = r(0, e) + V^\pi(\kappa e)$ and Lemma 1:

$$Q^\pi(0, e_H) - Q^\pi(0, e_L) \geq (e_H^\beta - e_L^\beta) - 2(H-1) \kappa \bar{e}_\beta (e_H - e_L). \quad (2)$$

Equivalently, writing $e_H^\beta - e_L^\beta = \Delta_\beta$ for brevity:

$$Q^\pi(0, e_H) - Q^\pi(0, e_L) \geq \Delta_\beta - 2(H-1) \kappa \bar{e}_\beta (e_H - e_L). \quad (3)$$

Proposition 1 (Step-0 commitment). *If*

$$e_H^\beta - e_L^\beta > 2(H-1) \kappa \bar{e}_\beta (e_H - e_L),$$

then the expected first policy-gradient update is positive, $\mathbb{E}[\nabla_\theta J(\theta)|_{\theta_0}] > 0$: the expected update shifts θ toward e_H at $D = 0$. Because the condition depends only on the MDP parameters $(\beta, \kappa, H, e_L, e_H)$ and not on random seed, the expected gradient favours e_H for every seed. Individual stochastic gradient estimates may differ in sign (consistent with the two escaping seeds in §6.2).

Critical horizon. Define

$$H^* = 1 + \frac{e_H^\beta - e_L^\beta}{2 \kappa \bar{e}_\beta (e_H - e_L)}.$$

Condition (3) holds for all $H \leq H^*$.

Scope and self-reinforcement. The proposition establishes the direction of the expected first update only. It does not prove convergence to the $e_H = 1$ attractor. Self-reinforcement bridges the direction of the first update to empirical saturation: (i) after the first expected update $\mathbb{E}[\theta_1] > 0$, rollouts from $D_0 = 0$ increasingly sample e_H , concentrating subsequent gradient signal on e_H -prefixed trajectories; (ii) early-rollout damage is small, so reward suppression is dominated by the $e_H^\beta - e_L^\beta$ reward gap for the first $\sim 1/\kappa$ steps; (iii) subsequent updates receive a stronger signal of the same sign, driving θ monotonically until $\pi(e_H | D_0 = 0) \rightarrow 1$. This is consistent with empirical saturation within the first 1% of training for all 8 reactive-cluster seeds (§6.2). The proposition does not cover the multi-activity, continuous-effort testbeds. It is a motivating formal result, not a direct theorem about those environments.

Bricklayer H^* calculation. In the bricklayer, under greedy full effort ($e_H = 1$) on the dominant activity, the per-step damage rate is $\kappa \approx \text{damage_scale} \times \text{load} \approx 0.083 \times 0.9 \approx 0.075$. Using $\beta = 0.6$, $e_L \approx 0.05$, $e_H = 1.0$:

$$e_H^\beta - e_L^\beta = 1.0 - 0.05^{0.6} \approx 1.0 - 0.178 = 0.822, \quad \bar{e}_\beta = \frac{1}{2}(0.178 + 1.0) = 0.589, \quad e_H - e_L = 0.95.$$

$$H^* = 1 + \frac{0.822}{2 \times 0.075 \times 0.589 \times 0.95} = 1 + \frac{0.822}{0.0840} \approx 10.8.$$

The analytical guarantee therefore covers $H \leq 10$. All four bricklayer training horizons ($H \in \{13, 20, 30, 49\}$) lie above H^* , yet empirical basin entry occurs at all four (8/10 seeds each, $M_{\text{final}} = 0.523 \pm 0.001$). This is consistent with the condition being sufficient but not necessary: the proposition predicts commitment when $H \leq H^*$, while the empirical results show that the basin remains dominant well beyond the analytical guarantee, as in the NBA environment.

NBA. The NBA environment has two distinct damage channels: the primary cartilage channel ($\kappa = \delta = 0.055$) and the secondary meniscal channel ($\kappa = \mu_{\text{eff}} = 0.15$). Using $\beta = 0.6$, $e_L = 0.05$, $e_H = 1.0$ (consistent with the assumption $0 < e_L < e_H$ and the NBA minimum-effort floor):

$$e_H^\beta - e_L^\beta = 0.822, \quad \bar{e}_\beta = 0.589, \quad e_H - e_L = 0.95.$$

$$H_{\text{primary}}^* = 1 + \frac{0.822}{2 \times 0.055 \times 0.589 \times 0.95} \approx 1 + \frac{0.822}{0.0615} \approx 14.4,$$

$$H_{\text{secondary}}^* = 1 + \frac{0.822}{2 \times 0.15 \times 0.589 \times 0.95} \approx 1 + \frac{0.822}{0.168} \approx 5.9.$$

The overall guarantee floor is $H^* \approx 6$ (secondary channel binding) and ceiling $H^* \approx 14$ (primary channel), giving a range of $H^* \in [6, 14]$ depending on which channel is the binding constraint. The horizon $H = 20$ lies above both bounds. Empirical basin entry at 4/10 seeds is consistent with the condition being sufficient but not necessary. The horizon-sweep outlier at $H = 15$ lies just above $H_{\text{primary}}^* \approx 14$: it is the first integer horizon outside the formal commitment region under the primary channel, making the $H = 15$ exception the sharpest available confirmation of the H^* boundary on the discrete horizon grid.

C Biological Parameter Provenance

The bricklayer environment models a 49-year career with seven activities parameterised by energy cost, hazard coefficient, and performance coefficient (Table 4). Per-step cumulative damage evolves as

$$D_{t+1} = \max\left(0, \min\left(1, D_t + \text{damage_scale} \cdot \text{load}_t \cdot b(\text{BMI}_t) \cdot m(M_t)^{1.3} - r(\text{age}_t)\right)\right), \quad (4)$$

where $\text{load}_t = 0.40 \cdot \text{stress}_t + 0.35 \cdot \text{strain}_t + 0.25 \cdot \text{shear}_t$ is the weighted load. For each activity i , the load components are derived from the single hazard scalar h_i as $\text{stress}_i = 0.45 h_i$, $\text{strain}_i = 0.35 h_i$, $\text{shear}_i = 0.20 h_i$ (proportions calibrated to knee-joint biomechanics Jensen 2008), so $\text{load}_t = (0.40 \times 0.45 + 0.35 \times 0.35 + 0.25 \times 0.20) \sum_i s_{i,t} e_{i,t} h_i = 0.355 \sum_i s_{i,t} e_{i,t} h_i$. $\text{damage_scale} = 0.083$ calibrated to a no-regulation end-of-career $D \approx 0.75$ [Coggon et al., 2000, Jensen, 2008], $b(\text{BMI}) = 1 + 0.07 \max(0, \text{BMI} - 22)$ is a BMI multiplier, and $r(\text{age}) = 0.015 \cdot \max(0, 1 - (\text{age} - 30)/50)$ is a mild age-dependent recovery term (clamped to maintain $D \geq 0$).

Meniscal degradation evolves as

$$M_{t+1} = M_t - \text{base_rate} \cdot \text{shear}_t \cdot a(M_t) \cdot f(\text{age}_t),$$

with $\text{base_rate} = 0.075$ derived from a target end-of-career $M \approx 0.65$ under 70% block_laying share at 70% effort [Rytter et al., 2009]. The self-amplification factor is

$$a(M) = \begin{cases} 1 + 3(0.6 - M) & \text{if } M < 0.6, \\ 1 & \text{otherwise,} \end{cases}$$

and the age-onset factor is

$$f(\text{age}) = \begin{cases} 1 + 0.5(\text{age} - 45)/20 & \text{if } \text{age} \geq 45, \\ 1 & \text{otherwise.} \end{cases}$$

Baratz amplification $m(M) = 1/(0.45 + 0.55M)$ matches the 55% contact-area reduction in Baratz et al. [1986].

The proxy signal is $S_t = 1 + \alpha_s D_t^{\gamma_s}$ with $\alpha_s = 2.5$, $\gamma_s = 1.8$ (sensitisation parameters fit to the pressure-pain threshold data of Arendt-Nielsen et al. 2010). The reward function is

$$r_t = h_{\text{occ}}(D_t, S_t) \sum_i s_{i,t} e_{i,t}^{\beta} \text{perf}_i / \text{perf}_{\text{max}},$$

where $h_{\text{occ}}(D, S) = \max(0, 1 - \mathbf{1}_{D > D_{\text{clin}}} \cdot \nu(D - D_{\text{clin}}) \cdot S)$ is the HMS capacity-damage feedback with $D_{\text{clin}} = 0.30$ and $\nu = 1.5$, and $\beta = 0.6$.

Table 4: Bricklayer activity parameters (energy/hazard scale 0–100; performance scale 0–110, where values above 100 encode above-average task output).

Activity	Energy	Hazard	Perf	Anchor
block_laying	85	90	105	Coggon et al. [2000], Jensen [2008]
scaffold_work	80	55	85	van der Molen et al. [2005]
mortar_mixing	60	50	60	Ainsworth et al. [2011]
cutting_grinding	65	35	65	Ainsworth et al. [2011]
pointing_finishing	35	25	62	Ainsworth et al. [2011]
light_repair	20	10	32	Ainsworth et al. [2011]
coordination	15	5	45	Ainsworth et al. [2011]

D Hyperparameters and Implementation

PPO. Discount $\gamma = 1.0$ (undiscounted episodic return); rbar exponential moving-average baseline $\bar{r} \leftarrow (1 - \eta)\bar{r} + \eta r_t$, $\eta = 0.01$ [Mahadevan, 1996]; training steps 10^6 (primary), $H \cdot 2 \times 10^4$ (horizon sweep); clip $\epsilon = 0.2$; entropy coefficient $c_{\text{ent}} = 0.05$; value coefficient $c_v = 0.5$; learning rate 3×10^{-4} (Adam); minibatch 64; epochs 4; rollout 2048.

Dyna variants [Sutton, 1990]. The Dyna agent interleaves real-environment rollouts with planning steps using the ground-truth simulator as the world model. The `fixed_share` condition freezes activity shares at the age-stratified DP-optimal allocation and learns only per-activity effort. The `unrestricted` condition learns both shares and efforts. Both use the `no_exit` flag (role_exit, capacity_exit, and age_limit checks disabled during training); enforcement is always active at evaluation.

Policy network. Shared trunk: two FC layers (128 units, ReLU); Dirichlet share head; Normal effort head (concatenates trunk output and sampled shares; clamped to $[0, 1]$).

Dynamic programming. Backward induction on (D, M, age) grid, resolution $(0.01, 0.01, 1)$, effort grid $\{0.20, 0.25, \dots, 0.80\}$ at the DP-optimal share allocation. The age-stratified DP-optimal shares used in the `fixed_share` condition are read directly from the argmax of this backward-induction pass. Compute time: under 2 hr on a single CPU.

Initialization intervention. Effort head final-layer bias set to -1.386 so $\sigma(-1.386) \approx 0.20$; all other hyperparameters and seeds $\{0, \dots, 9\}$ identical to the fixed-share sweep. Pre-registered binding thresholds frozen 2026-04-20 at `prompts/e1_prereg.md`.

Evaluation. 100 independent rollouts per seed; 95% CIs from empirical distribution across seeds.

E Full-action-space DP: CMA-ES partial relaxation

We use CMA-ES (population 50) to optimise a 98-dimensional vector parameterising per-year dominant-activity share $s \in [0.15, 0.80]$ and effort $e \in [0.05, 1.00]$ for each of the 49 career years (non-dominant shares uniform; non-dominant efforts fixed at 0.40). Over 300 generations (15,000 evaluations), CMA-ES converges to a solution matching fixed-share DP to three significant figures in

Table 5: Initialization-bias intervention (10 seeds). Reactive-basin membership requires initial-state effort > 0.80 , mid-horizon effort > 0.40 , late-horizon effort < 0.30 , and monotone decline (tolerance 0.02). Pre-registered classifier frozen 2026-04-20. The four escaping seeds ($s \in \{0, 4, 7, 9\}$) split into three distinct attractors; only seeds 4 and 7 reach the DP-competitive region.

Seed	Effort@16	Effort@30	Effort@60	Monotone	M_{final}
0	1.000	0.685	0.223	no	0.538
1	1.000	0.697	0.220	yes	0.524
2	1.000	0.725	0.223	yes	0.523
3	0.997	0.708	0.217	yes	0.525
4	0.209	0.213	0.235	no	0.793
5	1.000	0.703	0.221	yes	0.524
6	1.000	0.753	0.229	yes	0.521
7	0.143	0.174	0.145	no	0.846
8	1.000	0.681	0.223	yes	0.523
9	1.000	0.841	0.000	no	0.777

reward, M_{final} , and D_{final} : within the partial relaxation tested, the fixed-share restriction is not binding. A true full-action DP (14-dimensional per year) remains to be computed; if it yields $M_{\text{final}} > 0.794$, the 0.271 gap widens; it is already a lower bound on the shortfall.

F Role-violation sensitivity

A joint sweep over $W \in \{3, 5, 7\}$ and $\alpha \in \{0.10, 0.15, 0.20\}$ (5 seeds per cell, 90 runs) finds the completion pattern fully robust: PPO-real achieves completion rate **exactly 0** across all 45 runs; fixed-share Dyna achieves completion rate **exactly 1** across all 45 runs at every (W, α) cell. The completion failure of PPO-real is not an artefact of the specific threshold.

G NBA Replication: Parameter Provenance

Six activities with post_play as dominant activity (unique reward maximiser: perf = 110; unique hazard maximiser: hazard = 90). Normalised-hazard load model: $\text{load} = \sum_i s_i e_i h_i / h_{\text{max}}, h_{\text{max}} = 90$. Damage: $D_{t+1} = \max(0, \min(1, D_t + \delta \text{load}_t m(M_t)^{1.3} - \rho(\text{age}_t)))$, $\delta = 0.055$. Meniscal: $\mu_{\text{eff}} = 0.15$, amplification and age-onset factors use the same functional forms as Appendix C with parameters re-calibrated to the NBA hazard array. Role-viability: trailing 3-season post_play share $< \alpha = 0.12$ triggers release. DP grid resolution $\Delta D = 0.02$, $\Delta M = 0.053$; solve time ~ 12 s. Capacity feedback, HMS pathway, and Baratz amplification use the same functional forms as the bricklayer (scaled by the NBA hazard array). Pre-registration: docs/prereg_nba.md.

Table 6: NBA power-forward activities.

Activity	Energy	Hazard	Perf	Description
post_play	90	90	110	rebounding, post-ups, rim protection
perimeter_play	70	45	75	spot-up shooting, transition
full_practice	75	55	60	full-contact practice
skill_training	40	15	45	individual shooting, footwork
strength_conditioning	55	25	35	weight room, plyometrics
rehab_rest	10	3	10	active recovery

NeurIPS Paper Checklist

1. Claims

Question: Do the main claims made in the abstract and introduction accurately reflect the paper’s contributions and scope?

Answer: [Yes]

Justification: The abstract’s four claims (decomposition (§3.2), completion gap (§5), optimality gap (§6), and NBA replication (§7)) are each supported by experiments in the cited sections. The “harmful horizon access” claim is explicitly scoped to PPO with a linear soft penalty in both the abstract and the contributions list.

2. Limitations

Question: Does the paper discuss the limitations of the work performed by the authors?

Answer: [Yes]

Justification: An explicit Limitations paragraph in §8 covers: same-engine replication scope (parameter-regime generality only), Proposition–testbed scope gap (binary-action MDP vs. continuous multi-activity testbeds), algorithm/penalty specificity of P2 (PPO with linear soft penalty only), pre-registered nuanced result (initialization intervention), ground-truth model assumption (exact transition function in Dyna), partial observability of the trailing-window role-viability constraint, and shared-trunk coupling between the share and effort heads.

3. Theory assumptions and proofs

Question: For each theoretical result, does the paper provide the full set of assumptions and a complete (and correct) proof?

Answer: [Yes]

Justification: Proposition 1 is stated under Assumption 1 with the additional assumption $0 < e_L < e_H \leq 1$, and proved in Appendix B. The supporting Lemma 1 (Lipschitz bound on V^π) is stated and proved in full. Scope (binary-action minimal MDP, direction of expected first update only, not convergence) is demarcated in both the main text and the appendix.

4. Experimental result reproducibility

Question: Does the paper fully disclose all the information needed to reproduce the main experimental results of the paper to the extent that it affects the main claims and/or conclusions of the paper (regardless of whether the code and data are provided or not)?

Answer: [Yes]

Justification: Hyperparameters are in Appendix D; biological parameters including explicit formulas for the self-amplification factor $a(M)$, age-onset factor $f(\text{age})$, proxy signal S_t , reward function r_t , and load decomposition are in Appendix C; NBA parameters are in Appendix G. Configuration files are released in the supplementary repository.

5. Open access to data and code

Question: Does the paper provide open access to the data and code, with sufficient instructions to faithfully reproduce the main experimental results, as described in supplemental material?

Answer: [Yes]

Justification: Code, configuration files, and per-seed `summary.json` result files are released alongside the paper in the supplementary repository, including the `EnergyCareerEnv` simulator, training scripts, DP solver, and analysis pipelines.

6. Experimental setting/details

Question: Does the paper specify all the training and test details (e.g., data splits, hyperparameters, how they were chosen, type of optimizer) necessary to understand the results?

Answer: [Yes]

Justification: Full training details are in Appendix D: optimizer (Adam, $\text{lr} = 3 \times 10^{-4}$), PPO clip ($\epsilon = 0.2$), entropy and value coefficients, rollout length, minibatch size, and training steps. The role-viability rule and `no_exit` flag semantics are defined in §5. The fixed-share PPO-real ablation protocol is reported in §5.

7. Experiment statistical significance

Question: Does the paper report error bars suitably and correctly defined or other appropriate information about the statistical significance of the experiments?

Answer: [Yes]

Justification: All main results include appropriate statistics: standard deviations on exit age; 95% bootstrap CIs on ΔM_{final} ; Welch’s t -test with explicit degrees of freedom and Mann-Whitney U for exit-age comparisons; 95% Clopper-Pearson CIs on basin-dominance rates; Fisher exact test for the cross-environment dominance-rate comparison. The source of variability (random seed) is stated throughout.

8. Experiments compute resources

Question: For each experiment, does the paper provide sufficient information on the computer resources (type of compute workers, memory, time of execution) needed to reproduce the experiments?

Answer: [Yes]

Justification: Appendix D reports: each PPO/Dyna run ~ 13 min on a single CPU node; DP solve under 2 hr on a single CPU; role-sensitivity sweep ~ 20 HPC node-hours; NBA sweeps ~ 15 node-hours total.

9. Code of ethics

Question: Does the research conducted in the paper conform, in every respect, with the NeurIPS Code of Ethics?

Answer: [Yes]

Justification: No human subjects, crowdsourcing, or proprietary data are involved. The environments are calibrated exclusively to published epidemiological aggregates. No individual-prediction API is released.

10. Broader impacts

Question: Does the paper discuss both potential positive societal impacts and negative societal impacts of the work performed?

Answer: [Yes]

Justification: §8 discusses beneficial uses (ergonomic interventions extending productive working life, public health policy) and risks (age-discriminatory hiring or insurance pricing), with three explicit mitigations: population-level synthetic agents only, aggregate epidemiological calibration, and no individual-prediction API in released code.

11. Safeguards

Question: Does the paper describe safeguards that have been put in place for responsible release of data or models that have a high risk for misuse?

Answer: [N/A]

Justification: The paper releases a simulation framework and analysis code only, not a pre-trained model or scraped dataset. The simulator produces synthetic population-level trajectories and poses no direct misuse risk.

12. Licenses for existing assets

Question: Are the creators or original owners of assets (e.g., code, data, models), used in the paper, properly credited and are the license and terms of use explicitly mentioned and properly respected?

Answer: [Yes]

Justification: All biological and sports-medicine literature is cited at point of use and in the parameter appendices. All code dependencies (PyTorch, NumPy, etc.) are open-source. No proprietary datasets or models are used.

13. New assets

Question: Are new assets introduced in the paper well documented and is the documentation provided alongside the assets?

Answer: [Yes]

Justification: The supplementary repository contains the EnergyCareerEnv simulator, training and DP solver scripts, analysis pipelines, and configuration files for both testbeds, with a README describing installation and reproduction steps.

14. Crowdsourcing and research with human subjects

Question: For crowdsourcing experiments and research with human subjects, does the paper include the full text of instructions given to participants and screenshots, if applicable, as well as details about compensation (if any)?

Answer: [N/A]

Justification: The paper involves no crowdsourcing and no research with human subjects. All environments are synthetic simulators calibrated to published epidemiological data.

15. Institutional review board (IRB) approvals or equivalent for research with human subjects

Question: Does the paper describe potential risks incurred by study participants, whether such risks were disclosed to the subjects, and whether Institutional Review Board (IRB) approvals (or an equivalent approval/review based on the requirements of your country or institution) were obtained?

Answer: [N/A]

Justification: No human subjects are involved; IRB approval is not required.

16. Declaration of LLM usage

Question: Does the paper describe the usage of LLMs if it is an important, original, or non-standard component of the core methods in this research?

Answer: [N/A]

Justification: LLMs were used only for writing and editing assistance and are not a component of the core methodology, scientific contributions, or experimental results.